International Journal of Automotive Technology, Vol. ?, No. ?, pp. ?–?(year)

Estimation of Tire Lateral Force Using Adaptive Extended Kalman filter and Application to Adaptive Sliding Mode Control for Torque Vectoring

Jinmin Kim[1)], Hyunseup Jo[1)] and Sang Won Yoon[2)*]

[1)]Department of Automotive Engineering (Automotive – Computer Convergence), Hanyang University, Seoul 04763, Korea
[2)]Department of Electrical and Computer Engineering, Seoul National University, Seoul 08826, Korea

(*Received date ; Revised date ; Accepted date*)

ABSTRACT– In motorsports, precise and stable handling is crucial for a reliable driving. One solution is the use of a Torque Vectoring (TV) technique, which independently controls each wheel to generate yaw moment. TV systems require a design of a yaw rate controller; however, this enforces substantial challenges in Formula Student (FS) vehicles whose uncertainties and computational resources minimization are key concerns. This paper proposes design of a Sliding Mode Controller (SMC) as the yaw moment controller for FS vehicles. However, it has been reported that the switching term in the SMC introduced for robustness can adversely cause chattering problems. To address this issue, an adaptive SMC (ASMC) is introduced, which adjusts the switching term based on the estimation of lateral tire forces. These forces, which are influenced by diverse factors including tire cornering stiffness, are typically estimated using conventional models like Dugoff's tire model. This study employs an Adaptive Extended Kalman Filter (AEKF) for the lateral force estimation, coupled with an offline optimization to adjust cornering stiffness. The proposed approach is validated by coupling MATLAB/Simulink and CarMaker and evaluated in sinus steer and steady steer test. Simulation results demonstrate a notably improved handling accuracy with a significant reduction in chattering.

KEY WORDS: Adaptive sliding mode control, Adaptive extended kalman filter, Cornering stiffness, Formula student vehicle, Lateral tire force, Torque vectoring

NOMENCLATURE

v_x : longitudinal velocity, m/s
v_y : lateral velocity, m/s
γ : yaw rate, rad/s
a_x : longitudinal acceleration, m/s^2
a_y : lateral acceleration, m/s^2
δ : steering angle, rad
T_d : wheel driving torque, N·m
T_b : wheel braking torque, N·m
r : effective radius of tire, m
m : vehicle mass, kg
I_z : moment of inertia about z axis, kg·m^2
l_F : distance from front axle to the center of gravity, m
l_R : distance from rear axle to the center of gravity, m
L : wheel base length, m
t : half of track width, m
h : height from ground to the center of gravity, m
C_α : cornering stiffness, N/rad
σ : relaxation length, m
μ : road friction coefficient, -
α : slip angle, rad
F_x : longitudinal force between road and tire, N
F_y : lateral force between road and tire, N

SUBSCRIPTS

FL, FR, RL, RR: front left, front right, rear left, rear right

1. INTRODUCTION

Vehicle's performance in terms of acceleration, handling, and endurances are critical in racing, with high-speed cornering stability being essential. To enhance the handling performance of four in-wheel drive systems, controlling each motor individually for optimal torque distribution is effective (Shino *et al.,* 2001). This system is known as Torque Vectoring (TV) system, requiring the design of a yaw moment controller and various control strategies can be employed for this purpose. However, in Formula Student (FS) vehicle applications, two key considerations are essential: robustness and low

* *Corresponding author*. e-mail: swyoon@snu.ac.kr

computational power. The control system must operate robustly, especially since FS vehicles may be limited in their use of high-performance microcontrollers. Given these constraints, a Sliding Mode Controller (SMC) is introduced.

SMC works by forcing the system to slide along a predefined surface, defined by the sliding surface equation. Depending on the order of the sliding surface being controlled, it is referred to as First-Order Sliding Mode (FOSM) or Second Order Sliding Mode (SOSM). FOSM has the advantages of being simple to design and requiring low computational power. However, it can cause chattering problems, where the input value oscillates due to the switching term used for robustness. While SOSM effectively mitigates chattering issues, making it commonly applied to control systems for TV, it also enhances the system's robustness (Liang *et al*., 2020). However, FOSM, when combined with chattering reduction methods, provides sufficient performance for TV (de Carvalho Pinheiro *et al*, 2023). One of the methods is to adaptively change the switching gain during system operation, known as Adaptive Sliding Mode Control (ASMC) (Back *et al*., 2016). By adaptively adjusting the switching term based on the estimation of uncertainties, chattering can be prevented.

These uncertainties are concluded to the estimation of lateral tire forces, which are influenced by various factors such as slip angle, road conditions, vertical load, and the tire's cornering stiffness. Given the complexity of these interactions, precise modeling techniques are necessary for reliable tire force estimation. Dugoff's tire model is one of the commonly used approach due to its simplicity in combining both lateral and longitudinal tire forces based on slip angle and slip ratio (Dugoff *et al*., 1970). However, a major limitation of this model is the assumption that cornering stiffness remains a constant value. This assumption can lead to inaccuracies in lateral force estimation, especially at higher slip angles, where the tire's behavior deviates from the model's linearity. To address this, previous studies have explored the nonlinear relationship between the lateral force and cornering stiffness (Baffet *et al.,* 2009; Doumiati *et al*., 2011; Jeong *et al*., 2022). On the other hand, an alternative approach has been proposed that estimates lateral tire force without relying on conventional tire models or filtering methods (Li *et al*., 2019). Instead, they predict the lateral tire force directly by focusing on the distribution of vertical load across the tires relative to the total load on certain axle.

Thus, this study is divided into two main parts. Firstly, we employed the Adaptive Extended Kalman Filter (AEKF) for lateral force estimation and coupled it with an offline optimization approach to adjust cornering stiffness using the vertical load distribution method. Secondly, TV system, which is following neutral steer yaw rate using ASMC that adjusts the switching gain based on the uncertainties estimated by the AEKF. Experiments are conducted in CarMaker to validate both the AEKF and ASMC approaches.

2. ESTIMATION OF LATERAL TIRE FORCE

In this section, the lateral force estimation process using an Adaptive Extended Kalman Filter (AEKF) is described, along with an introduction to an offline optimization approach for modifying cornering stiffness. The estimation process consists of three main parts: (1) the vehicle lateral dynamics model under the three degrees of freedom (3-DoF), (2) vertical force calculation, and (3) a brief explanation of Dugoff's tire model, which is widely used for its simplicity. The detailed four-wheel vehicle model is illustrated in Figure 1, and the equations of vehicle dynamics are formulated as follows (Doumiati *et al.*, 2011; Lee *et al*., 2018):

$$\begin{aligned}\dot{v}_x = \frac{1}{m}\{&F_{x,FL}\cos(\delta_{FL}) + F_{x,FR}\cos(\delta_{FR}) - \cdots \\ &F_{y,FL}\sin(\delta_{FL}) - F_{y,FR}\sin(\delta_{FR}) + F_{x,RL} + \cdots \\ &F_{x,RR} - C_{air}V_x^2\} + v_y\gamma\end{aligned} \tag{1}$$

$$\begin{aligned}\dot{v}_y = \frac{1}{m}\{&F_{x,FL}\sin(\delta_{FL}) + F_{x,FR}\sin(\delta_{FR}) + \cdots \\ &F_{y,FL}\cos(\delta_{FL}) + F_{y,FR}\cos(\delta_{FR}) + \cdots \\ &F_{y,RL} + F_{y,RR}\} + v_x\gamma\end{aligned} \tag{2}$$

$$\begin{aligned}\dot{\gamma} = \frac{1}{I_z}[&l_F\{F_{x,FL}\sin(\delta_{FL}) + F_{x,FR}\sin(\delta_{FR}) + \cdots \\ &F_{y,FR}\cos(\delta_{FL}) + F_{y,FR}\cos(\delta_{FR})\} - \cdots \\ &l_R(F_{y,RL} + F_{y,RR}) + \cdots \\ &t\{F_{x,FL}\cos(\delta_{FL}) - \cdots \\ &F_{x,FR}\cos(\delta_{FR}) - F_{y,FL}\sin(\delta_{FL}) + \ldots \\ &F_{y,FR}\sin(\delta_{FR}) + F_{x,RL} - F_{x,RR}\}]\end{aligned} \tag{3}$$

where v_x, v_y, γ, δ_{FL}, δ_{FR}, m, I_z, l_F, l_R, t, C_{air} are the longitudinal velocity, lateral velocity, yaw rate, front left wheel steering angle, front right wheel steering angle, vehicle mass, moment of inertia about yaw axis, distance from front axle to the center of gravity (CG), distance from rear axle to the CG, half of track width and aerodynamic drag resistance, respectively. Tire forces, $F_{x,i}$ and $F_{y,i}$ (i denotes the axle position) represent the longitudinal and lateral forces with the subscript (FL, FR, RL, RR).

Lateral forces on the tire generated by the interaction with the road surface are primarily due to the presence of a slip angle. Therefore, calculating the slip angle is critical for determining lateral tire forces; this can be calculated as described in Eq. (4).

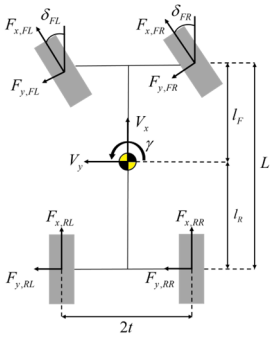

Figure 1. Representation of a four-wheel vehicle model.

$$\begin{aligned}
\alpha_{FL} &= \delta_{FL} - \tan^{-1}\left(\frac{v_y + l_F\gamma}{v_x}\right) \\
\alpha_{FR} &= \delta_{FR} - \tan^{-1}\left(\frac{v_y + l_F\gamma}{v_x}\right) \\
\alpha_{RL} &= -\tan^{-1}\left(\frac{v_y - l_R\gamma}{v_x}\right) \\
\alpha_{RR} &= -\tan^{-1}\left(\frac{v_y - l_R\gamma}{v_x}\right)
\end{aligned} \tag{4}$$

where δ_{FL}, δ_{FR} denotes the front left wheel steering angle and front right wheel steering angle.

2.1. Vertical tire force calculation

The vertical tire force (F_z) plays a crucial role in accurately estimating lateral forces. It is essential to account for F_z through that consider load transfer and acceleration, as these are directly influenced during the vehicle's dynamic behavior such as cornering, accelerating, and braking.

The couplings between pitch and roll dynamics are neglected in this study, assuming these have a minimal effect on the overall vertical force calculation. The vertical forces can be simplified and calculated using the approach as outlined in Eq. (5) (Doumiati *et al.*, 2011).

$$\begin{aligned}
F_{z,FL} &= mg\frac{l_R}{2L} - m\frac{h}{2L}a_x - m\frac{hl_R}{tL}a_y \\
F_{z,FR} &= mg\frac{l_R}{2L} - m\frac{h}{2L}a_x + m\frac{hl_R}{tL}a_y \\
F_{z,RL} &= mg\frac{l_R}{2L} + m\frac{h}{2L}a_x - m\frac{hl_F}{tL}a_y \\
F_{z,RR} &= mg\frac{l_R}{2L} + m\frac{h}{2L}a_x + m\frac{hl_F}{tL}a_y
\end{aligned} \tag{5}$$

where m, g, h, t, L, a_x, a_y are the vehicle mass, gravitational acceleration, distance from ground to CG, half of track width, wheelbase length, longitudinal acceleration and lateral acceleration, respectively.

2.2. Dugoff's tire model

To represent tire forces, Dugoff's tire model combines both lateral and longitudinal tire forces. It calculates these forces based on the slip ratio of longitudinal forces and the slip angle for lateral forces. By neglecting longitudinal slip ratio, simplified Dugoff's tire model for lateral force is described in Eq. (6).

$$\begin{aligned}
\bar{F}_{y,i} &= -C_{\alpha,i}\tan(\alpha_i) f(\lambda_i) \\
f(\lambda_i) &= \begin{cases} (2-\lambda_i)\lambda_i, & \text{if } \lambda_i < 1 \\ 1, & \text{if } \lambda_i \geq 1 \end{cases} \\
\lambda_i &= \frac{\mu F_{z,i}}{2C_{\alpha,i}\,|\tan(\alpha_i)|}
\end{aligned} \tag{6}$$

where $C_{\alpha,i}$ represent the cornering stiffness of each axle, and μ is the tire-road friction coefficient, assumed to be 1.0 for a high-friction road surface. (Dugoff *et al*., 1970). Meanwhile, the lateral force is generated with a time lag relative to change in slip angle, it causes transient response of the tire. The lateral tire force dynamics is first order and represented as follows (Guenther *et al*., 1990, Heydinger *et al*., 1991):

$$\dot{F}_{y,i} = \frac{v_x}{\sigma_i}(-F_{y,i} + \bar{F}_{y,i}) \tag{7}$$

Here, σ denotes the relaxation length, which is assumed to be constant value of 0.1m in this study.

2.3 Axle distribution based-lateral force

As mentioned before, the Dugoff's tire model assumes that the lateral tire force is proportional to slip angle. However, this assumption is only valid within a limited small range of slip angle. As slip angle increases, the behavior of the tire becomes nonlinear and no longer increases proportionally with the slip angle. Instead, it approaches a saturation point where further increases in slip angle yield diminishing lateral tire force. Thus, predicting lateral tire force using linear models becomes less accurate.

On the other hand, the lateral tire force can be predicted directly by focusing on the distribution of vertical load across the tires relative to the total load on certain axle (Li *et al*., 2019). The equations for calculating lateral tire force based on axle load distribution are described in Eqs. (8), (9).

$$\begin{aligned}
\tilde{F}_{y,FL} &= \frac{F_{z,FL}}{F_{z,FL}+F_{z,FR}}F_{y,F} \\
\tilde{F}_{y,FR} &= \frac{F_{z,FR}}{F_{z,FL}+F_{z,FR}}F_{y,F} \\
\tilde{F}_{y,RL} &= \frac{F_{z,RL}}{F_{z,RL}+F_{z,RR}}F_{y,R} \\
\tilde{F}_{y,RR} &= \frac{F_{z,RR}}{F_{z,RL}+F_{z,RR}}F_{y,R}
\end{aligned} \tag{8}$$

$$F_{y,i} = m\frac{L-l_i}{L}a_y, i = F, R \tag{9}$$

Here, $\tilde{F}_{y,i}$ represents the lateral tire force, $F_{y,F}$ and $F_{y,R}$ are the total lateral forces on the front and rear axles, respectively.

2.4. Optimization for modifying cornering stiffness

According to T. D. Gillespie, load transfer affects cornering stiffness, and this relationship can be presented by a second-order polynomial with respect to vertical force. The second-order polynomial equation is adjusted by adding a bias term ($C_{\alpha 0}$) in this study as described in Eq. (10), where $C_{\alpha 0}$ represents the initial cornering stiffness when side slip angle is small. While the axle distribution-based method does not fully capture the nonlinear relationship between lateral force and slip angle, it remains effective for modifying the cornering stiffness and reflecting nonlinear changes as the slip angle increases.

$$C_\alpha(F_z) = aF_z^2 + bF_z + C_{\alpha 0} \tag{10}$$

$$F_{y,i} = -C_{\alpha,i}(F_{z,i})\cdot\alpha_i \tag{11}$$

To further refine cornering stiffness, an optimization problem is then formulated aimed at reflecting the effect of vertical load, as defined in Eq. (12). This involves minimizing the sum of squared error between Eq. (8) and Eq. (11).

$$\min_{[a,b]} \sum_i \| \tilde{F}_{y,i} - (-(aF_{z,i}^{\ 2} + bF_{z,i} + C_{\alpha 0})\alpha_i) \|^2 \tag{12}$$

The Levenberg Marquardt method is utilized for this optimization task and the optimal values for the coefficients a, b are -0.006 and 3.501, respectively.

2.5. Adaptive extended kalman filter

To estimate the lateral force in state-space model, the AEKF is employed to dynamically adjust the process noise (Akhlaghi *et al*., 2017). Unlike the process noise, which is adjusted dynamically to reflect changes in the system state transitions, the measurement noise is kept constant and remain relatively stable under normal operating conditions. The AEKF utilizes 8-dimensional state vector (x_k), 5-dimensional input control vector (u_k), and 5-dimenstional measurement vector (z_k) as follows:

$$\begin{cases}
x_k = [v_x, v_y, \gamma, F_{y,FL}, F_{y,FR}, F_{y,RL}, F_{y,RR}]^T \\
u_k = [\delta = \dfrac{(\delta_{FL}+\delta_{FR})}{2}, F_{x,FL}, F_{x,FR}, F_{x,RL}, F_{x,RR}]^T \\
z_k = [v_x, v_y, \gamma, a_x, a_y]^T
\end{cases} \tag{13}$$

$$F_{x,i} = \frac{\tau_{d,i} - \tau_{b,i}}{r} \tag{14}$$

$F_{x,i}$ is excluded from the state vector and used as an input control vectors, calculated using Eq. (14). These values are determined by using the wheel driving torque, wheel braking torque, and the effective radius of the tire denoted as $\tau_{d,i}, \tau_{b,i}, r$, respectively.

The state transition model, and the measurement model are described in Eqs. (15), (16). where $\hat{x}_k^-$ represent the priori state, ω_k is the Gaussian noise during state transition at the discrete time step *k*. While z_k represent the measurement affected by υ_k, which is also Gaussian noise at the discrete time step *k*.

$$\hat{x}_k^- = f(\hat{x}_{k-1}, u_k) + \omega_k \tag{15}$$

$$z_k = h(\hat{x}_k^-) + \upsilon_k \tag{16}$$

The detailed description of $f(\cdot)$ and $h(\cdot)$ are described in Eqs. (18), (19). Meanwhile, compared to conventional EKF process, the AEKF adaptively adjust the system noise covariance matrix (Q) by balancing the weight (ρ, set to 0.65) between the Q_{k-1} and the innovation (d_k) term. This adjustment is necessary because the measurement noise remains relatively consistent, while the system noise (e.g., F_x in this study) is often difficult to quantify accurately. The entire process of AEKF is outlined in Eq. (17).

$$\begin{cases}
\hat{x}_k^- = f(\hat{x}_{k-1}, u_k) \\
P_k^- = F_k P_{k-1} F_k^{\ T} + Q_{k-1} \\
K_k = P_k^- H_k^{\ T} (H_k P_k^- H_k^{\ T} + R)^{-1} \\
d_k = z_k - h(\hat{x}_k^-) \\
\hat{x}_k = \hat{x}_k^- + K_k d_k \\
Q_k = \rho \cdot Q_{k-1} + (1-\rho)\cdot(K_k d_k d_k^{\ T} K_k^{\ T})
\end{cases} \tag{17}$$

Here, *P, Q,* and *R* represent the state covariance matrix, system noise covariance, and measurement noise covariance. *F, H* are the Jacobian matrices of the $f(\cdot)$ and $h(\cdot)$, respectively.

$$f = \begin{bmatrix} \frac{1}{m}\{F_{x,FL}\cos(\delta_{FL}) + F_{x,FR}\cos(\delta_{FR}) - \cdots \\ F_{y,FL}\sin(\delta_{FL}) - F_{y,FR}\sin(\delta_{FR}) + F_{x,RL} + \cdots \\ F_{x,RR} - C_{air}V_x{}^2\} + v_y\gamma \\ \frac{1}{m}\{F_{x,FL}\sin(\delta_{FL}) + F_{x,FR}\sin(\delta_{FR}) + \cdots \\ F_{y,FL}\cos(\delta_{FL}) + F_{y,FR}\cos(\delta_{FR}) + F_{y,RL} + \cdots \\ F_{y,RR}\} + v_x\gamma \\ \frac{1}{I_z}[l_F\{F_{x,FL}\sin(\delta_{FL}) + F_{x,FR}\sin(\delta_{FR}) + \cdots \\ F_{y,FR}\cos(\delta_{FR}) + F_{y,FR}\cos(\delta_{FR})\} - \cdots \\ l_R(F_{y,RL} + F_{y,RR}) + t\{F_{x,FL}\cos(\delta_{FL}) - \cdots \\ F_{x,FR}\cos(\delta_{FR}) - F_{y,FL}\sin(\delta_{FL}) + \ldots \\ F_{y,FR}\sin(\delta_{FR}) + F_{x,RL} - F_{x,RR}\}] \\ \frac{v_x}{\sigma}(-F_{y,FL} + \bar{F}_{y,FL}) \\ \frac{v_x}{\sigma}(-F_{y,FL} + \bar{F}_{y,FL}) \\ \frac{v_x}{\sigma}(-F_{y,FR} + \bar{F}_{y,FR}) \\ \frac{v_x}{\sigma}(-F_{y,RR} + \bar{F}_{y,RR}) \end{bmatrix} \Delta t \quad (18)$$

$$h = \begin{bmatrix} v_x \\ v_y \\ \gamma \\ \frac{1}{m}\{(F_{x,FL} + F_{x,FR})\cos(\delta) - \cdots \\ (F_{y,FL} + F_{y,FR})\sin(\delta) + \cdots \\ (F_{x,RL} + F_{x,RR}) - (C_{air}v_x{}^2)\} \\ \frac{1}{m}\{(F_{x,FL} + F_{x,FR})\sin(\delta) + \cdots \\ (F_{y,FL} + F_{y,FR})\cos(\delta) + \cdots \\ (F_{y,RL} + F_{y,RR})\} \end{bmatrix} \quad (19)$$

3. TORQUE VECTORING SYSTEM

For the TV system, an Adaptive Sliding Mode Control (ASMC) approach is utilized for the yaw moment controller to ensure robustness. There are several techniques reducing chattering problem, such as incorporating a low-pass filter or replacing the signum function with a saturation function. While adding a low-pass filter can help minimize chattering, it negatively affects the controller's performance (De Carvalho Pinheiro *et al.,* 2023). Therefore, this study employs the saturation function along with the adaptive switching gain to mitigate chattering problem.

3.1. Sliding Mode Controller Design

To establish SMC for torque vectoring, the sliding surface is designed for the vehicle's yaw rate to track the desired yaw rate. it is expressed as follows:

$$S = \gamma - \gamma_{des} \quad (20)$$

The process of setting the control input involves following two steps. First, establish the equivalent control, which ensures $S = 0$ under the assumption of no disturbances and can be determined by imposing derivation of S is zero. Meanwhile, derivation of yaw rate is defined in Eq. (3). This can be partitioned into two components: one is M_x, which consist of F_x, and the other is M_y, which consists of F_y, as described in the following equations:

$$\dot{S} = \dot{\gamma} - \dot{\gamma}_{des} = 0 \quad (21)$$

$$\begin{aligned} M_x = {} & \{F_{x,FR}\cos(\delta_{FR}) - F_{x,FL}\cos(\delta_{FL})\}t + \cdots \\ & \{F_{x,FL}\sin(\delta_{FL}) + F_{x,FR}\sin(\delta_{FR})\}l_F + \cdots \\ & (F_{x,RR} - F_{x,RL})t \end{aligned} \quad (22)$$

$$\begin{aligned} M_y = {} & \{F_{y,FL}\sin(\delta_{FL}) - F_{y,FR}\sin(\delta_{FR})\}t + \cdots \\ & \{F_{y,FL}\cos(\delta_{FL}) + F_{y,FR}\cos(\delta_{FR})\}l_f - \cdots \\ & (F_{y,RR} + F_{y,RL})l_R \end{aligned} \quad (23)$$

Using above equations, the derivatives of S can be substituted as follows:

$$\dot{S} = \frac{1}{I_z}(M_x + M_y + M_d) - \dot{\gamma}_{des} = 0 \quad (24)$$

where M_d is added to represent disturbances. The term M_x, which can be controlled using braking and acceleration, is treated as a control input. M_y is associated with lateral forces that are difficult to achieve. for getting equivalent control input, neglecting M_d and M_y, the equivalent control input defined Eq. (25) (Liang *et al*., 2020; de Carvalho Pinheiro *et al*., 2023; Zhang *et al*., 2020; Goggia et al., 2014).

$$u_{eq} = I_z \dot{\gamma}_{des} \tag{25}$$

Signum function is incorporated into the control input as a switching term. However, the signum function can be replaced by a saturation function to reduce the chattering phenomenon (Truong *et al*., 2013). Consequently, the control input is defined as follows:

$$u = I_z \dot{\gamma}_{des} - K \cdot sat(S) \tag{26}$$

where K is the control gain for sliding mode control. To ensure the sliding surface converges in finite time, Lyapunov functions are used. According to Eq. (28) and Eq. (29), the control gain must be over the $M_d + M_y$.

$$\mathrm{V} = \frac{1}{2} S^2 \tag{27}$$

$$\begin{aligned} \dot{\mathrm{V}} &= S\dot{S} \\ &= S\,\{\frac{1}{I_z}(I_z \dot{\gamma}_{des} - K \cdot sat(S) + \cdots \\ &\quad M_y + M_d) - \dot{\gamma}_{des}\} \\ &= S\,\{-\frac{K}{I_z} sat(S) + \frac{1}{I_z}(M_d + M_y)\} \\ &\quad \le -\frac{K}{I_z} S \cdot sat(S) + \frac{|S|}{I_z}(M_d + M_y) \\ &\quad \le |S|\{-K + M_d + M_y\} \le 0 \end{aligned} \tag{28}$$

Based on the results of the AEKF and the sliding surface, an adaptively adjusted switching gain is employed to establish the reference value, accounting for uncertainties. The AEKF results are utilized as indicators of the magnitude of the uncertainty. The proposed equation is as follows:

$$K_{AEKF} = A\left\lceil \left| \frac{\tilde{M}_y}{A} \right| \right\rceil + B \tag{29}$$

$\tilde{M}_y$ is the estimation of M_y using the AEKF. The absolute value of estimation value is divided by a tunable variable A, and the result is rounded up using ceiling operator ($\lceil \cdot \rceil$). This rounded value is then multiplied by A again. This approach ensures that the gain mitigating the influence of oscillations in the AEKF results while remaining within its upper bounds. Additionally, a bias term B is added to account for any additional disturbances or uncertainties not captured by the initial estimate.

The method of adjusting switching gain based on the states of sliding variable effectively addressed chattering phenomena near the sliding manifold (Back *et al*., 2016). To prevent setting the excessive switching gain, a weight that reflects switching gain. This weight is managed according to the following rules:

1) If the sliding variable is smaller than in the previous step. It is assumed sliding gain is appropriate. The weight is not updated and prevent divergence, if the sliding variable reaches a predefined maximum value, the weight is not updated.
2) If the sliding variable is larger than in the previous step, it indicates the need for a higher gain, prompting an increase in the update step.
3) If the sliding variable's sign has changed compared to the previous step, it suggests system convergence. The weight is updated to smaller
4) If there is a change in K_{AEKF}, it is regarded as a change in the environment. To handle this condition, the weight of switching gain is reset to 1.

Following these rules, the weight update can express as follows:

$$w_k = \begin{cases} w_{k-1} & with\ |s_{k-1}| > |s_k|\ or\ w_{k-1} > 2 \\ w_{k-1}(1-\theta) & with\ s_k s_{k-1} < 0 \\ w_{k-1}(1+\theta) & with\ |s_{k-1}| < |s_k| \\ 1 & with\ K_{AEKF,k-1} \neq K_{AEKF,k} \end{cases} \tag{30}$$

where w is weight, θ is tunable variable that determines the amount of change in each step. Consequently, switching gain K is Eq. (31)

$$K = w_t * K_{AEKF} \tag{31}$$

3.2. Torque Distribution

The desired momentum is generated using FOSM. To achieve this momentum, the vehicle utilizes both steering and torque distribution. The ratio of torque distribution can be calculated by optimization-based control-allocation to achieve a specific purpose or by distributing it equally (De Novovellis *et al*., 2013). While optimization-based control allocation can enhance the vehicle's performance, we choose to distribute torque equally to minimize computational resources. However, the force generated by the drivetrain has limitations. If the power distribution exceeded a motor's maximum capacity, it cannot maintain speed. In such case, the excess power is redistributed to the other motors.

4. EXPERIMENT AND RESULTS

The overall process of lateral force estimation, offline cornering stiffness optimization, and TV system are illustrated in Fig. 2. Our approach is tested using the

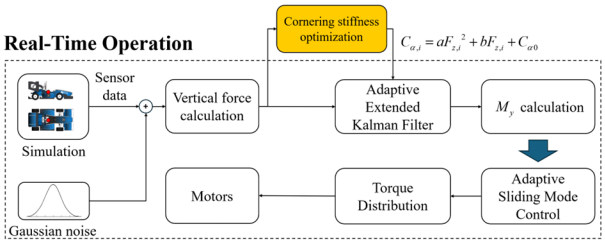

Figure 2. Overall system diagram.

CarMaker simulation environment. The tests are conducted on a FS vehicle, equipped with virtual GNSS and Inertial Measurement Unit (IMU) sensor that had Gaussian noise added to simulate real-world inaccuracies, providing a more realistic evaluation of the proposed method. Two distinct scenarios were employed to assess its effectiveness in estimating lateral forces and TV. The two test scenarios include:

1) Sinus steer test: this is commonly used to assess the response of a vehicle to rapidly varying steering angles. The specific conditions involved driving the vehicle at a constant speed of 40km/h, with a sinusoidal steering input ranging from $-100°$ to $100°$ over a 5-second period
2) Steady steer test: this test represents a steady-state cornering condition. The vehicle maintained a speed of 45km/h while driving on a circular track with a road curvature 45 meters.

4.1 AEKF Results

The results of estimated lateral forces and M_y during the test scenarios are shown in Fig. 3 (sinus steer test) and Fig. 4 (steady steer test). The blue line represents the ground truth achieved by CarMaker, while the orange line shows our result. The root mean square error (RMSE) values are summarized in Table 1. Although consistent errors remain in both tests, they are small enough to be used for mitigating uncertainty in the ASMC.

Table 1. RMSE results for lateral force in each test

	$F_{y,FL}$ (N)	$F_{y,FR}$ (N)	$F_{y,RL}$ (N)	$F_{y,RR}$ (N)	M_y (Nm)
Sinus	94.73	106.11	74.44	65.71	78.24
Steady	78.22	66.75	47.22	67.93	30.63

The results indicate that the RMSE values for the front lateral forces are consistently higher than those for the rear in both tests. This is attributed to the front axles experiencing more variation due to the steering input,

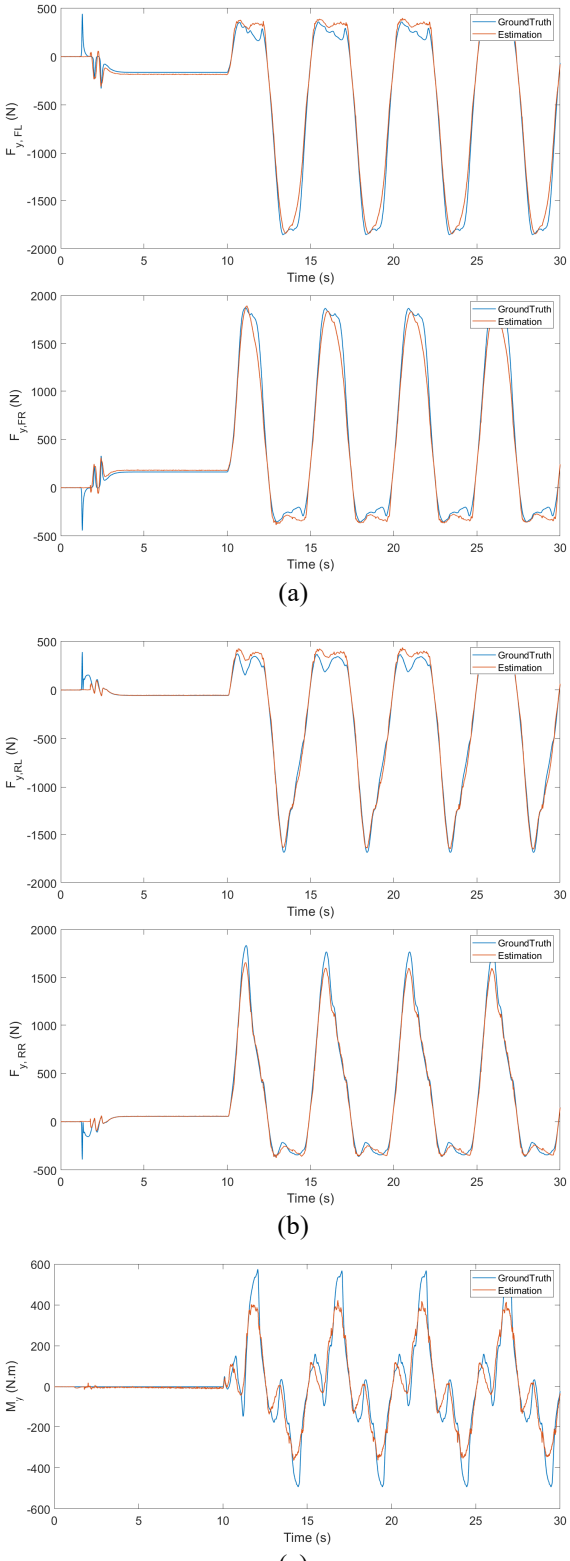

Figure 3. Estimation results achieved from the sinus steer test. (a) $F_{y,F}$, (b) $F_{y,R}$, and (c) M_y.

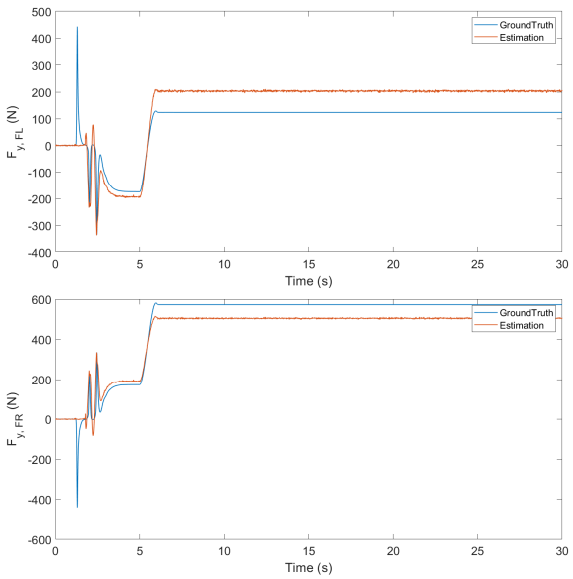

(a)

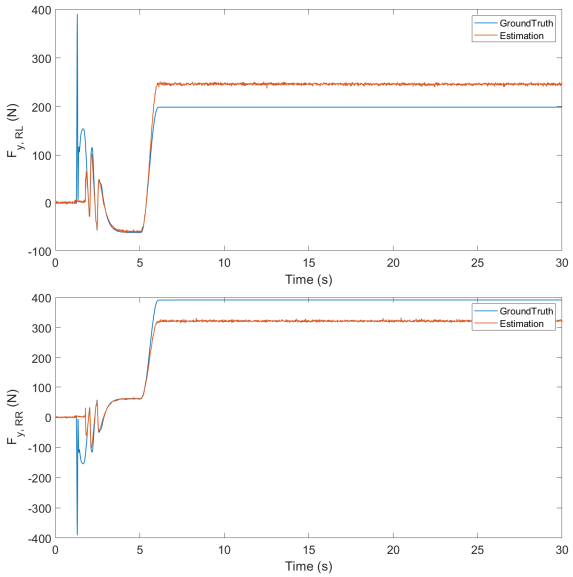

(b)

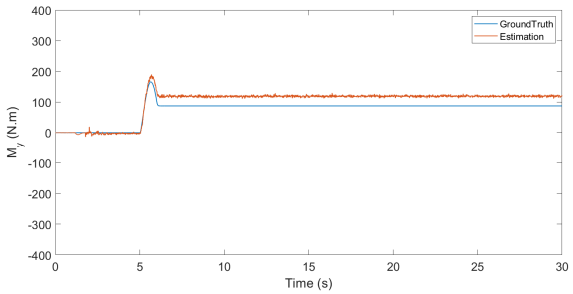

(c)

Figure 3. Estimation results achieved from the steady steer test. (a) $F_{y,F}$, (b) $F_{y,R}$, and (c) M_y.

resulting in increased errors. Moreover, the RMSE values for the sinus steer test are consistently higher than those for the steady steer test. This is due to the sinus steer test involving rapid, continuous changes in the steering angle, leading to dynamic behavior in the overall vehicle's lateral forces.

4.2. Torque Vectoring Results

We evaluate whether the controller follows the desired yaw rate and compare the effects of torque vectoring with the benchmark scenario that torque vectoring is not applied. The desired yaw rate is set according to vehicle's neutral steer condition that is calculated by driver's steering angle. In this simulation, the tuning of the variable A, B, and θ defined in Eq. (29) is as follows:

1) A: This parameter must be set considering the error of the AEKF. In section 4.1, the AEKF's error during both test scenarios does not exceed 500 Nm, and the adaptive term, w can make the switching gain up to double. Therefore, A is set to 500 to cover maximum 1000.
2) B: The value of B should consider the disturbance torque, M_d. However, M_d was not estimated in this paper. To ensure robustness, the control gain must be set to above this term. To achieve this, the lateral forces, and longitudinal forces that offered Carmaker are used to calculate yaw moments M_x and M_y. According to Eq. (3), the multiply by inertia moment and derivation of yaw moment comprises M_y and M_x. The differences between these values can be interpreted as M_d. Fig. 5 shows the result for M_d on the, where M_d does not exceed 500Nm. Thus, B is set to 500.
3) θ: The time step for updating the weight is set to 10 milliseconds in this simulation. If θ is set too high, the weight changes would occur too rapidly. For stability, θ is conservatively set to 0.01.

Fig. 6 shows the results of the desired yaw rate and the vehicle's yaw rate during the sinus steer test. The blue, yellow, and orange lines represent the desired yaw rate,

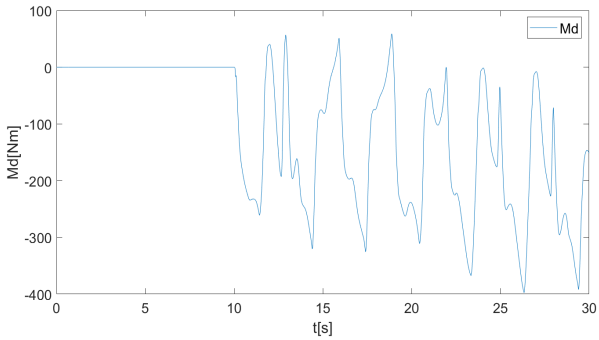

Figure 5. Result of M_d.

benchmark technique without torque vectoring (TV), and our process including TV. The figure shows that, using the benchmark results without TV, the vehicle's yaw rate is limited by its own characteristics. However, with TV, the vehicle's yaw rate closely follows the desired yaw rate.

The steady steer test results are displayed Fig. 7. Different from Fig. 6, our TV process exhibits a chattering issue at the transition around 5 to 10 seconds due to the SMC's limitation, and the amplitude of chattering diminishes as time elapses thanks to the adjusted switching gain. However, as shown in Fig. 8. after 15 seconds, the red and blue lines are similar, but the yellow line is different from the desired yaw rate.

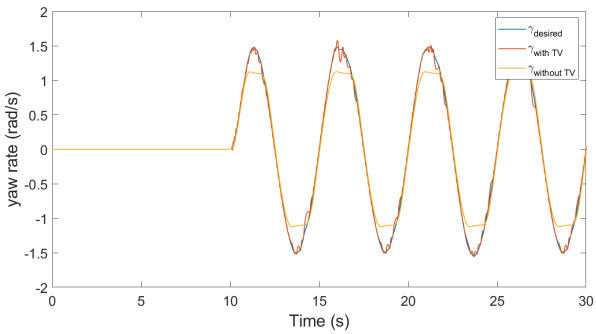

Figure 6. Yaw rate for the vehicles with and without TV system in sinus steer test.

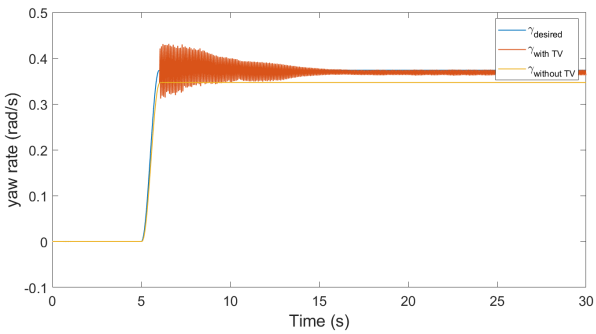

Figure 7. Yaw rate for the vehicles with and without TV system in steady steer test.

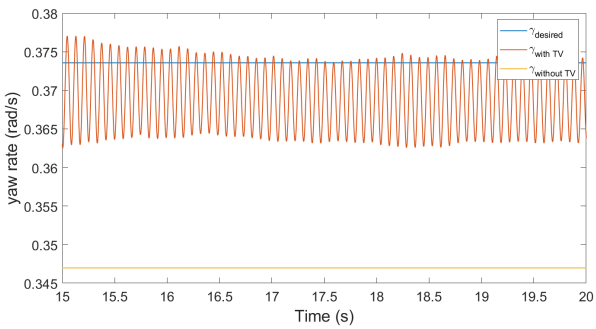

Figure 8. 15 to 20 sec in sinus steer test.

5. CONCLUSTION

This paper proposes a Torque-Vectoring system with an Adaptive Sliding Mode Controller (ASMC), coupled with an Adaptive Extended Kalman Filter (AEKF) for estimating tire lateral forces, to enhance handling performance in Formula Student vehicles. For the AEKF, an offline optimization method to adjust cornering stiffness is introduced to improve accuracy, and estimation results are then utilized to adjust the switching term of the ASMC and generates a yaw moment. Our results demonstrated that the AEKF provided highly accurate estimations in both sinus and steady steer tests. The TV system successfully tracked the desired yaw rate in both the sinus and steady steer tests. The sinus steer test demonstrated that the proposed controller effectively followed the desired yaw rate. However, in the steady steer test, a chattering problem was observed when the sliding manifold became saturated. Nonetheless, due to adjustments in switching gain, the system was able to its states, which reduced the chattering problem. Consequently, the proposed method proved effective in managing the FS vehicle system.

ACKNOWLEDGEMENT– This work was supported by Institute of Information & communications Technology Planning & Evaluation (IITP) grant funded by the Korea government (MSIT) (No.2022-0-01053, Development of Network Load Balancing Techniques Based on Multiple Communication/Computing/Storage Resources)

REFERENCES

Akhlaghi, S., Zhou, N. and Huang, Z., (2017), July. Adaptive adjustment of noise covariance in Kalman filter for dynamic state estimation. In *2017 IEEE power & energy society general meeting,* 1-5.

Baek, J., Jin, M., and Han, S. (2016). A new adaptive sliding-mode control scheme for application to robot manipulators. IEEE *Transactions on industrial electronics*, **63, 6**, 3628-3637.

Baffet, G., Charara, A. and Lechner, D., (2009). Estimation of vehicle sideslip, tire force and wheel cornering stiffness. *Control Engineering Practice,* **17**, **11**, 1255-1264.

De Carvalho Pinheiro, H., Carello, M., and Punta, E. (2023). Torque vectoring control strategies comparison for hybrid vehicles with two rear electric motors. *Applied Sciences,* **13**, **14**, 8109.

De Novellis, L., Sorniotti, A.,and Gruber, P. (2013). Wheel torque distribution criteria for electric vehicles with torque-vectoring differentials. *IEEE transactions on vehicular technology*, **63**, **4**, 1593-1602.

Dugoff, H., Fancher, P.S. and Segel, L., (1970). An analysis of tire traction properties and their influence

on vehicle dynamic performance. *SAE transactions*, 1219-1243.

Goggia, T., Sorniotti, A., De Novellis, L., Ferrara, A., Gruber, P., Theunissen, J., Steenbeke, D., Knauder,B. and Zehetner, J. (2014). Integral sliding mode for the torque-vectoring control of fully electric vehicles: Theoretical design and experimental assessment. *IEEE Transactions on Vehicular Technology*, **64**, **5**, 1701-1715.

Heydinger, G.J., Garrott, W.R. and Chrstos, J.P., (1991). The importance of tire lag on simulated transient vehicle response. *SAE transactions*, 362-374.

Jeong, D., Ko, G. and Choi, S.B., (2022). Estimation of sideslip angle and cornering stiffness of an articulated vehicle using a constrained lateral dynamics model. *Mechatronics*, **85**, 102810.

Lee, E., Jung, H. and Choi, S., (2018). Tire lateral force estimation using Kalman filter. *International Journal of Automotive Technology*, **19**, 669-676.

Li, L., d'Andréa-Novel, B. and Thorel, S., (2019), October. New online estimation algorithm of lateral tire-road coefficients based on Inertial Navigation System. In *2019 IEEE Intelligent Transportation Systems Conference (ITSC),* 3859-3866.

Liang, J., Zhao, J., Dong, Z., Wang, Y. and Ding, Z. (2020). Torque Vectoring and Rear-Wheel-Steering Control for Vehicle's Uncertain Slips on Soft and Slope Terrain Using Sliding Mode Algorithm. *IEEE Transactions on Vehicular Technology,* **69**, **4**, 3805-3815.

Loeb, J.S., Guenther, D.A., Chen, H.H.F. and Ellis, J.R., (1990). Lateral stiffness, cornering stiffness and relaxation length of the pneumatic tire. *SAE transactions*, 147-155.

Truong, D. T., Meywerk, M., and Tomaske, W. (2013). Torque vectoring for rear axle using Adaptive Sliding Mode Control. *2013 international conference on control, automation and information sciences (ICCAIS),* 328-333.

Zhang, L., Ding, H., Shi, J., Huang, Y., Chen, H., Guo, K., and Li, Q. (2020). An adaptive backstepping sliding mode controller to improve vehicle maneuverability and stability via torque vectoring control. *IEEE Transactions on Vehicular Technology*, **69**, **3**, 2598-2612.